

## Corrosion Performance of Fe-Al Intermetallic Coatings in 1.0 M NaOH Solution

J. Porcayo-Calderon<sup>1,\*</sup>, C.D. Arrieta-Gonzalez<sup>2</sup>, A. Luna-Ramirez<sup>3</sup>, V.M. Salinas-Bravo<sup>3</sup>,  
C. Cuevas-Arteaga<sup>1</sup>, A. Bedolla-Jacuiende<sup>4</sup> and L. Martinez-Gomez<sup>5</sup>

<sup>1</sup>Universidad Autonoma del Estado de Morelos, CIICAp, Av. Universidad 1001, 62209-Cuernavaca, Morelos, Mexico

<sup>2</sup>Instituto Tecnológico de Zacatepec, Calzada Tecnológico 27, C.P. 62780, Zacatepec, Morelos, Mexico.

<sup>3</sup>Instituto de Investigaciones Eléctricas, 62490-Cuernavaca, Mor., México, Reforma 113, Col. Palmira, 62490, Cuernavaca, Morelos, México.

<sup>4</sup>Instituto de Investigaciones Metalúrgicas-UMSNH, Ciudad Universitaria, Morelia, Michoacán, MEXICO.

<sup>5</sup>Universidad Nacional Autónoma de México, Instituto de Ciencias Físicas, Av. Universidad s/n, Cuernavaca, Morelos, Mexico

\*E-mail: [jporcayoc@gmail.com](mailto:jporcayoc@gmail.com)

Received: 16 July 2013 / Accepted: 22 August 2013 / Published: 25 September 2013

---

Three different particle sizes were used to deposit FeAl and Fe<sub>3</sub>Al intermetallic coatings by thermal spray techniques: flame spraying and HVOF (High Velocity Oxygen Fuel). Coatings were characterized by SEM (scanning electron microscopy) and their characteristics are presented considering particle size and deposition process employed. Coatings performance was evaluated using electrochemical test in a solution of 1.0 M NaOH at room temperature. It was observed that deposition technique used and particle size influences the electrochemical performance of coatings. Coatings showed no significant variations in their current densities, but were one order of magnitude higher than those of base alloys, the corrosion potential of coatings were similar regardless of the particle size and more active than their alloy base.

---

**Keywords:** Intermetallics, Iron aluminides, Coatings, Thermal spraying, Corrosion

### 1. INTRODUCTION

Intermetallic phases based on the high activity of aluminum have very attractive properties as low density, high melting point, high thermal conductivity, excellent oxidation, hot corrosion resistance and good mechanical properties [1]. Intermetallic compounds have potential use in systems requiring excellent behavior of materials in aggressive environments such as steam generators and

coal-fired gas turbine because of its high resistance to high temperature oxidation and lower density compared to conventional Fe and Ni based alloys. However, these compounds continue to face various challenges mainly concerning its resistance to high and low temperature ductility. While achieving a solution to these problems, another field of progress of these materials is to use its oxidation resistance at high temperature through its application as coatings on structural materials with poor properties of oxidation and corrosion resistance [2].

Use of intermetallic compounds as surface layer appears to be an attractive alternative and different routes have been proposed to get them through diffusional processes, thermal spraying and sputtering among others [1]. However, from a production standpoint, there are only three methods for use in protective coatings: chemical vapor deposition (CVD) by pack diffusion, physical vapor deposition (PVD), and thermal spraying. The pack diffusion process has the disadvantage of possible inclusion of particles in the coating pack which can cause failure of the coating and is a process that cannot be used on site and is expensive. The PVD is a complex process which includes the deposition of multicomponent coatings as required to take into account the vapor pressures of all elements to produce a chemistry controlled of the alloy. Coatings deposited by thermal spray processes have improved properties compared with those obtained by CVD and PVD processes, also they do not affect the substrate properties, it offers greater productivity and their implementation costs are lower [3].

The thermal spray process is a viable method for the deposition of a variety of materials and is an attractive technique. Several studies report the use of this process for the application of intermetallic compounds where these alloy powders were obtained from inert gas atomization [2, 4], atomization in an inert atmosphere with subsequent milling [5-7], mechanical alloying [8-9] and synthesis by self-propagating high temperature [1]. Few studies have been reported where the intermetallic powder obtained from the pulverization of the ingot [10]. Deposition techniques of intermetallic coatings are as diverse as HVOF thermal spraying [1-2, 4-7, 11-18], electro-welding [19] and plasma spraying [4, 8-10].

Additionally, although iron aluminides have been developed primarily for high temperature structural applications because of their ability to develop an  $\text{Al}_2\text{O}_3$  protective layer that provides corrosion resistance to molten salt environments [20], their excellent performance in these conditions has motivated its study in aqueous solutions. It is therefore of interest to know their properties of corrosion resistance in aqueous acidic and basic media and in media rich in chloride and sulfur compounds [21].

This paper reports on the performance of Fe-Al coatings using HVOF and flame spraying processes, respectively. Coatings were sprayed onto stainless steel substrate. Coatings were characterized in terms of microstructure and evaluated in terms of their corrosion resistance.

## **2. EXPERIMENTAL PROCEDURE**

### *2.1. Materials*

Intermetallic alloys were obtained by fusion of high purity metallic elements (> 99.99%) in the corresponding stoichiometric ratios for  $\text{Fe}_3\text{Al}$  and  $\text{FeAl}$  compounds. The fusions were performed in an

induction furnace under inert atmosphere, and subsequently were cast in molds to form rods. As cast intermetallic alloys were ground in a hammer mill to a particle size less than 3 mm in diameter, and later pulverized in a ball mill. The grinding time for a batch of 2 kg was 8 days and achieved a particle size smaller than 200 mesh. Afterwards, powder alloys were classified according to their particle size in a vibrating mesh. Table 1 shows the chemical elemental composition, determined by atomic absorption spectroscopy of the powder alloys. The coatings were deposited from three different particles sizes. It was defined as coarse particle size to the powder alloys with particle size between 56-84  $\mu\text{m}$ , medium particle size to the powder alloys between 56-41  $\mu\text{m}$ , and fine particle size to the powder alloys with particle size less than 41  $\mu\text{m}$ .

## 2.2. Thermal spray processes

The coatings were deposited on a 304 stainless steel substrate and two thermal spray processes were used: a) projection of powders by oxyacetylene flame and b) HVOF process (High Velocity Oxygen-Fuel). For the first case a Sulzer-Metco gun 5PII model was utilized, in this case the powder alloy is gravity fed into a stream of compressed air and conveyed to a suspended oxyacetylene flame where it is heated to a molten or semi-molten state and then is projected onto the substrate to form the coating. For the HVOF process, a Sulzer-Metco model DJ2700 was utilized. The flame was generated by the combustion of a propane-oxygen mixture; in this case, the velocity of particles is greater than 500 m/s. Because of the high kinetic energy of particles, coatings deposited have high density and low porosity. Table 2 and 3 show the parameters for the different spray application techniques. The same working conditions for all three particle sizes tested were applied. Prior to coating application, samples were cleaned with acetone and superficially prepared by grit blast according to the NACE standard 1/SSPC-SP No. 5. Afterwards were degreased with acetone and ready for application of coatings.

**Table 1.** Elemental chemical composition of the intermetallic alloys powder.

Powder alloy	Concentration (weight %)	
	Al	Fe
Fe <sub>3</sub> Al	12.86	87.14
FeAl	27.62	72.38

**Table 2.** Powder flame spraying process parameters.

Parameter	Value
Oxygen Pressure (kPa)	273
Acetylene pressure (kPa)	201
Oxygen flow rate (m <sup>3</sup> /h)	1.7
Acetylene flow rate (m <sup>3</sup> /h)	0.93
Drag the powders	gravity
Nozzle	P7B-G
Spraying distance	18-20 cm
Atmospheric spray	Air

**Table 3.** HVOF process parameters.

Parameter	Value
Oxygen Pressure (kPa)	1135
Propane Pressure (kPa)	790
Air Pressure (psi)	618
Oxygen flow rate (m <sup>3</sup> /h)	16
Propane flow rate (m <sup>3</sup> /h)	4.4
Air flow rate (m <sup>3</sup> /h)	21
Carrier gas	Nitrogen
Carrier gas pressure (kPa)	963
Spraying distance	18-20 cm
Atmospheric spray	Air

### 2.3. Corrosion test

The corrosion resistance of the coatings was evaluated by potentiodynamic polarization testing, measurement of open circuit potential ( $E_{corr}$ ) and linear polarization resistance (LPR). A three-electrode electrochemical cell was utilized, the reference electrode was a saturated calomel electrode (SCE), the counter electrode was a platinum wire, and as a working electrode the coatings and intermetallic alloys. Intermetallic alloys and coatings were evaluated in a 1.0 M NaOH solution at room temperature without aeration for 30 days. Potentiodynamic polarization tests were conducted from -300 mV to 2000 mV with respect to its corrosion potential ( $E_{corr}$ ) and a scan rate of 60 mV/min. RPL measurements were performed at a scanning rate of 10 mV/min respect to  $E_{corr}$ .

## 3. RESULTS AND DISCUSSION

### 3.1. Characterization of powder alloys and coatings

Figure 1 shows the X-ray diffraction patterns for the intermetallic powder alloys. The peaks observed correspond to the Fe<sub>3</sub>Al and FeAl intermetallic alloys and they are consistent with those reported by other authors [6, 22, 23]. The width of the peaks is related to the size reduction in the powder grain and with the presence of stresses due to plastic deformation occurring during milling [24].

Figures 2 and 3 show the cross section of FeAl and Fe<sub>3</sub>Al coatings deposited by the powder flame spray process and by HVOF process, respectively. The micrographs show the effect of different particle sizes on the final coating obtained. In general, it appears that the coatings exhibit a lamellar structure. Coatings obtained by powder flame spray process (Figure 2) show the presence of pores (Figure 2a), partially melted particles (Figure 2c) with the initial appearance of the powder particle [25], partially fractured particles due to particle impact velocity with the surface and trapped oxides [7, 18] (dark phases), and some partially oxidized particles (Figure 2b) can be observed. These features are seen in all cases regardless of the particle size of the feedstock.

By contrast, the coatings produced by the HVOF process, Figure 3, show a denser coat (Figure 3c), with lower porosity, been more uniform and homogeneous. Fewer oxidized particles and unmelted particles can be observed. These are typical characteristics of coatings applied by the HVOF process, due to the high kinetic energy of the particles upon impact. In case of coatings deposited from coarse particle size powder, it is observed that not all the particles reach an energy state to allow its complete deformation upon impact, and hence their cohesion with the other particles was low. This was observed because during metallographic preparation of the coatings some particles were detached from the coat.

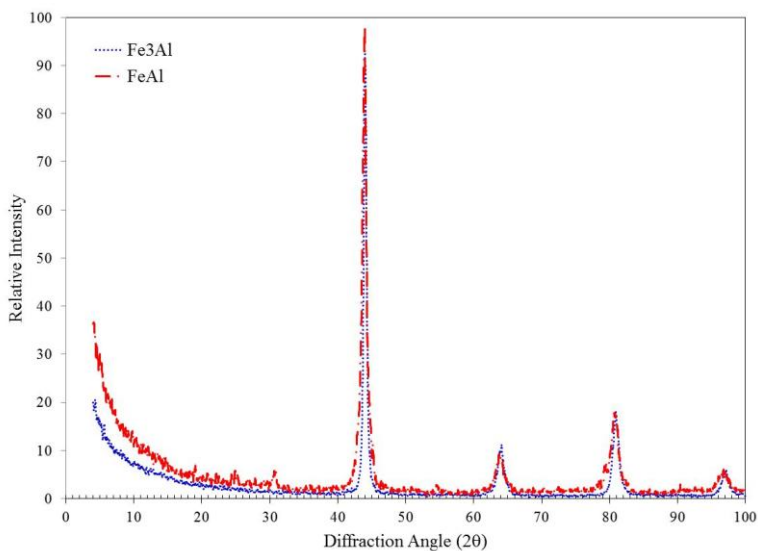


Figure 1. The X-ray diffraction patterns of FeAl and Fe<sub>3</sub>Al powder alloys.

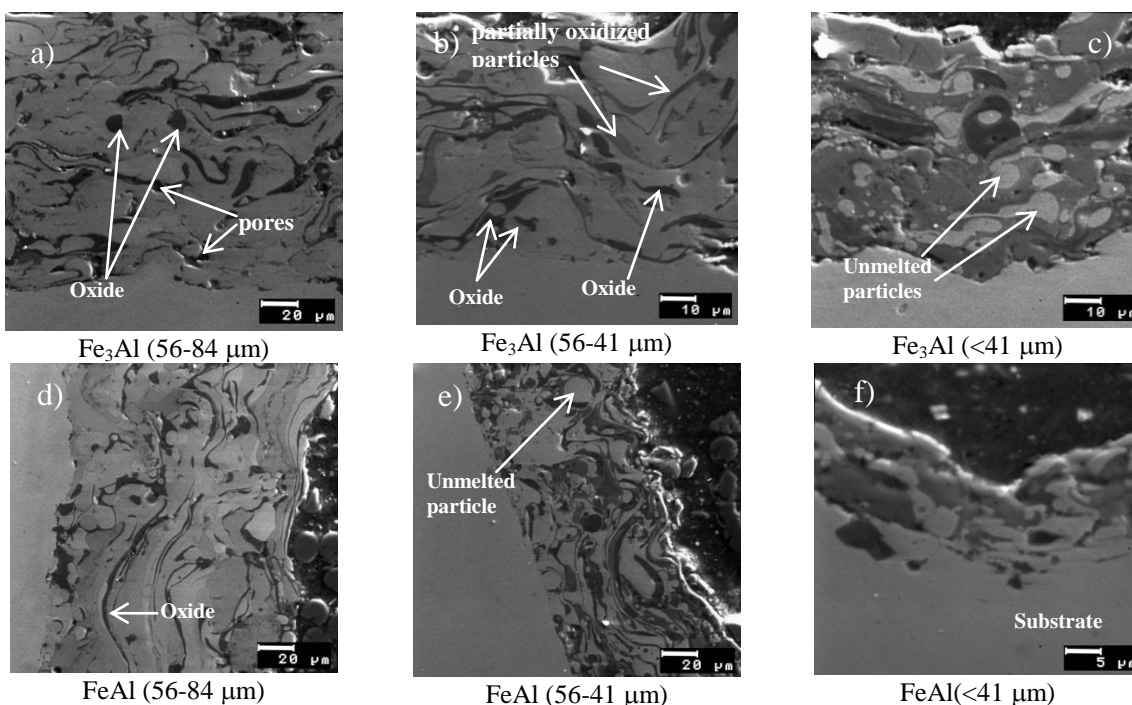
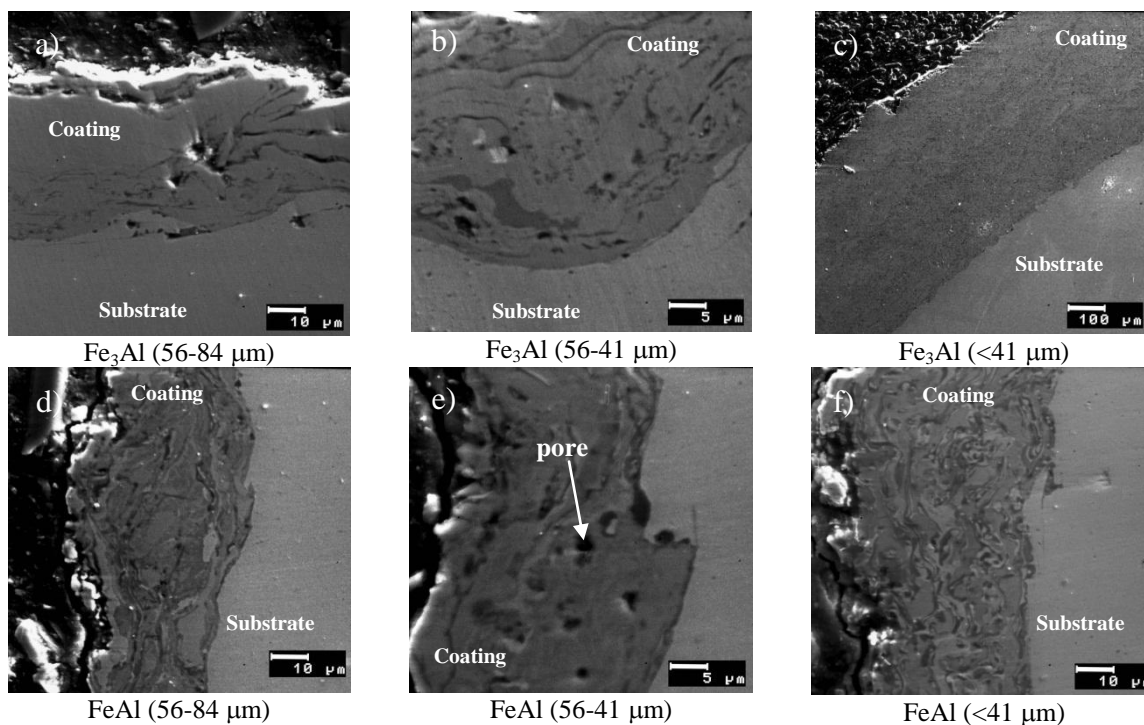


Figure 2. Cross section of FeAl and Fe<sub>3</sub>Al coatings deposited by the powder flame spray process.



**Figure 3.** Cross section of FeAl and Fe<sub>3</sub>Al coatings deposited by HVOF process.

Coatings obtained with medium and fine particle size show better characteristics than similar coatings applied by the powder flame spray process, an important difference to note it is the low presence of trapped oxides.

Coatings deposited by the powder flame spray process show considerable porosity, oxides, and a high fraction of unmelted. By contrast, the coatings produced by HVOF process exhibit lower porosity and a very low fraction of trapped oxides. It has been stated that the unmelted particles fraction decreases as the particle speed is increased [26]. This is consistent with the microstructural characteristics of the coatings deposited by both processes. Similar observations have been reported in previous research on this type of coatings [6, 26, 27].

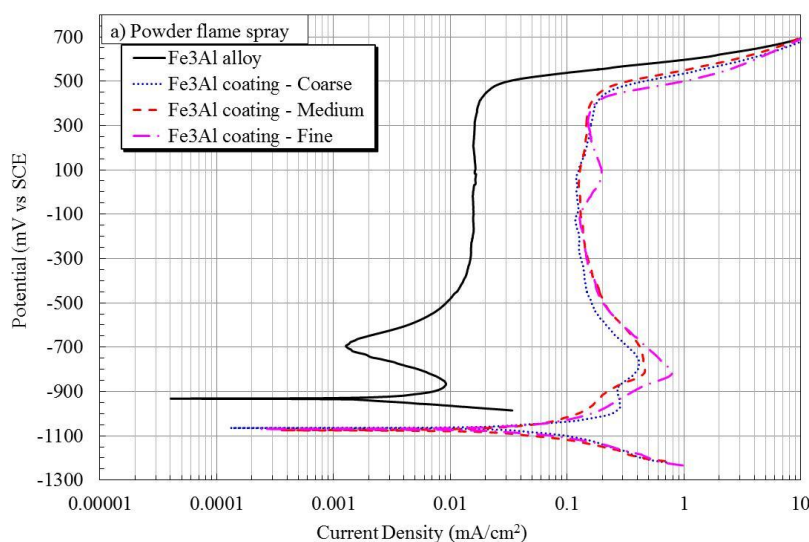
### 3.2. Electrochemical measurements

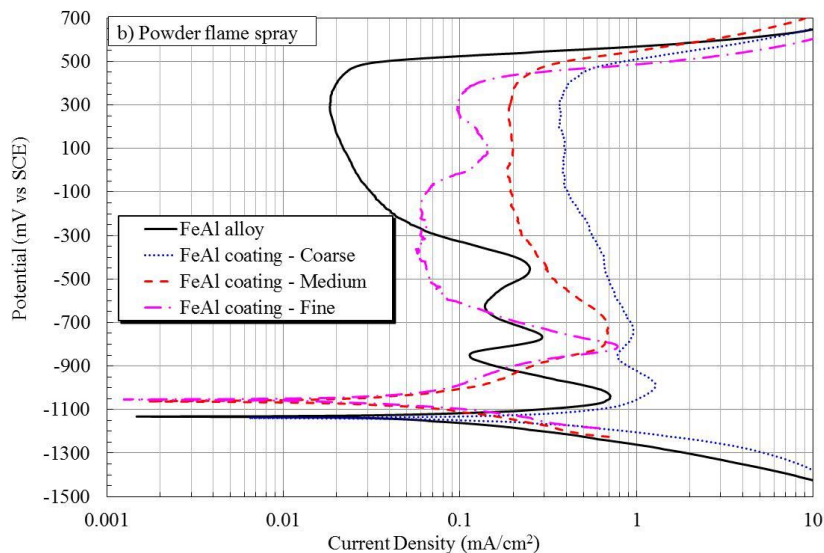
#### 3.2.1. Polarization tests

Figure 4 shows the potentiodynamic polarization curves for intermetallic alloys and intermetallic coatings deposited by powder flame spraying process. It's noted that all the alloys and coatings show a typical active-passive-transpassive behavior. In the case of coatings Fe<sub>3</sub>Al (Figure 4a), it is noted that regardless of particle size, all coatings showed a similar behavior, showing a passive region between -800 and 400 mV and a similar values of current density. These values are higher than those of the base alloy Fe<sub>3</sub>Al. The corrosion potential of the Fe<sub>3</sub>Al alloy is nobler than that of the coatings and the anodic branch exhibits a passive region between -400 and 400 mV, with a current density value lower than that of the coatings. FeAl coatings (Figure 4b) show a similar behavior than

its base alloy. Coatings with medium and fine grain size show the lowest  $I_{corr}$  values. Both coatings and alloy displayed a similar passive region. FeAl base alloy shows a passive zone formed by two regions, where the first one begins at -1060 mV, and it is characterized by the presence of several increments and decrements in current density up to -470 mV. Then begins a second passive region until 320 mV where a transpassive zone starts. Tables 4 and 5 show the electrochemical parameters obtained from polarization curves for intermetallic alloys and coatings deposited by powder flame spray process.

Figure 5 shows the polarization curves of the coatings deposited by the HVOF process. In case of Fe<sub>3</sub>Al coatings exhibit (figure 5a) a similar behavior between them, but their  $E_{corr}$  values are more active than the base alloy, also the  $I_{corr}$  values are higher. The Fe<sub>3</sub>Al coating of coarse particle size showed the highest corrosion rate. The range of the passive zone of the coating is between 400 and -800 mV, with a transpassive region between 400 and 500 mV. FeAl coatings and base alloy have a similar behavior, but the coatings show higher corrosion rates. In this case, FeAl coating with coarse particle size showed the highest corrosion rate. All coatings show a passive region between -950 and 450 mV, but at higher current densities than the base alloy. Table 6 shows the electrochemical parameters obtained from polarization curves. In general,  $I_{corr}$  values of coatings were higher compared to those of the base alloy, and this is consistent with other studies about iron aluminide coatings [7] and other materials such as stainless steel [28, 29] and titanium [30]. This behavior can be attributed to two factors: the surface finish and the Al content. It is known that in its as-deposited condition, the coatings have greater surface area due to their roughness and porosity, and these factors can affect the calculated values from electrochemical measurements [31]. In addition, Man et al. [32] indicate that a metal or alloy cannot adequately build a passive layer on a rough surface. Furthermore, it is known that the Al content determines the formation of a passive and compact protective layer [33, 34]. In the case of the base alloy its Al content contributes to the formation of a protective layer, and on the contrary, the coatings experience a loss of aluminum during the spraying process. This may influence the formation of a passive film rich in Al [7]. In base alloys, the presence of two stages in the passivation regions may be related to the presence of two oxide layers, an external Fe-rich oxide layer, and an inner Al-rich oxide layer [7].





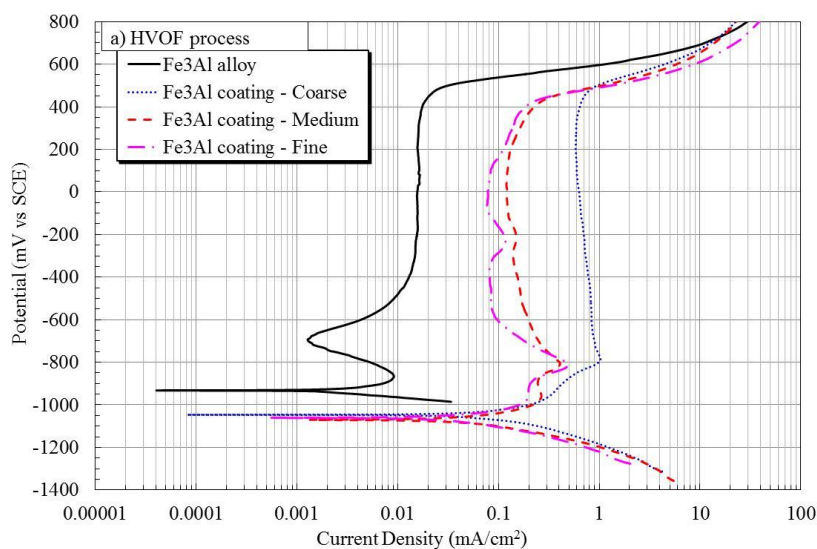
**Figure 4.** Polarization curves for a) Fe<sub>3</sub>Al coatings and base alloy, and b) FeAl coatings and base alloy, deposited by the powder flame spray process in 1.0 M NaOH at 25°C.

**Table 4.** Electrochemical parameters for the Fe<sub>3</sub>Al and FeAl base alloys in 1.0 M NaOH at 25°C.

Alloy	$E_{corr}$ (mV)	$I_{corr}$ (mA/cm <sup>2</sup> )	$\beta_a$	$\beta_c$
Fe <sub>3</sub> Al	-932	0.0036	99	52
FeAl	-1132	0.16	106	155

**Table 5.** Electrochemical parameters for the Fe<sub>3</sub>Al and FeAl coatings deposited by the powder flame spray process in 1.0 M NaOH at 25°C.

Coating	Coarse particle size				Medium particle size				Fine particle size			
	$E_{corr}$ (mV)	$I_{corr}$ (mA/cm <sup>2</sup> )	$\beta_a$	$\beta_c$	$E_{corr}$ (mV)	$I_{corr}$ (mA/cm <sup>2</sup> )	$\beta_a$	$\beta_c$	$E_{corr}$ (mV)	$I_{corr}$ (mA/cm <sup>2</sup> )	$\beta_a$	$\beta_c$
Fe <sub>3</sub> Al	-1064	0.07	123	171	-1074	0.07	290	156	-1069	0.08	260	160
FeAl	-1138	0.73	450	185	-1061	0.08	253	183	-1053	0.06	251	115



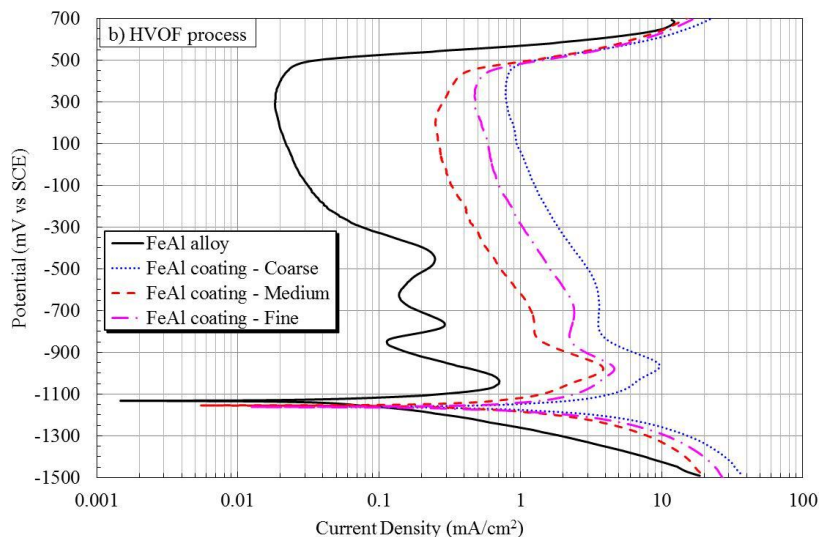


**Figure 5.** Polarization curves for a) Fe<sub>3</sub>Al coatings and base alloy, and b) FeAl coatings and base alloy, deposited by the HVOF process in 1.0 M NaOH at 25°C.

**Table 6.** Electrochemical parameters for the Fe<sub>3</sub>Al and FeAl coatings deposited by the HVOF process in 1.0 M NaOH at 25°C.

Coatings	Coarse particle size				Medium particle size				Fine particle size			
	<i>E</i> <sub>corr</sub> (mV)	<i>i</i> <sub>corr</sub> (mA/cm <sup>2</sup> )	β <sub>a</sub>	β <sub>c</sub>	<i>E</i> <sub>corr</sub> (mV)	<i>i</i> <sub>corr</sub> (mA/cm <sup>2</sup> )	β <sub>a</sub>	β <sub>c</sub>	<i>E</i> <sub>corr</sub> (mV)	<i>i</i> <sub>corr</sub> (mA/cm <sup>2</sup> )	β <sub>a</sub>	β <sub>c</sub>
Fe <sub>3</sub> Al	-1046	0.15	307	163	-1070	0.07	157	114	-1060	0.07	162	128
FeAl	-1162	2.8	415	212	-1154	1.1	252	135	-1162	2.7	480	183

### 3.2.2. Corrosion potential measurements

Figures 6 and 7 show the variation of *E*<sub>corr</sub> measurements for 30 days for Fe<sub>3</sub>Al and FeAl alloys and coatings, respectively. Determination of the chemical interaction of metallic materials with the electrolyte is essential in order to understand their stability and their active-passive behavior. One simple way to study the film formation and passivation of metallic materials in a solution is to monitor the *E*<sub>corr</sub> as a function of time. A rise of potential in the positive direction indicates the formation of a passive film, and a steady potential indicates that the film remains intact and protective. A drop of potential in the negative direction indicates breaks in the film, dissolution of the film, or no film formation [35].

Fe<sub>3</sub>Al coatings and alloy tend to increase their *E*<sub>corr</sub> values in the first 24 hours of immersion. The increase in *E*<sub>corr</sub> values can be associated with factors that favor the growth of diffusion layers which alter the surface activity such as adsorption of ions, oxide formation, oxide dissolution, as well as changes in the concentration of metal ions and oxygen [17, 36]. After 24 hours of immersion, all coatings with medium and fine particle size showed a steady increase in their *E*<sub>corr</sub> values, reaching values higher than those of their base alloy. This may be related to the stability of the passive layer formed on the coating surface [37]. The coatings deposited with coarse size particle showed a different

behavior, in this case, their  $E_{corr}$  values were lower their alloy base. This behavior may be explained because the electrolyte has permeated through the porosity of the coating reaching the surface of the substrate, or because the active-passive behavior of the coating surface [17, 37].

The coatings of medium and fine particle size deposited by powder thermal spraying process, and the coating of fine particle size deposited by HVOF process, and the FeAl alloy (Figure 7) showed a rapid increase in its corrosion potential during the first 24 hours of immersion. Afterwards  $E_{corr}$  values increase slightly and remain practically unchanged until the end of the test. This behavior is related to the stability of the passive layer formed on the coating [37]. The coating of fine particle size deposited by HVOF process showed a stable potential during the first 10 days of immersion, and suddenly changed to more noble values (-350 mV), and remained constant until the end of the test. Also the coating of coarse particle size deposited by flame spray showed the same behavior but its potential increase after 20 days of immersion.

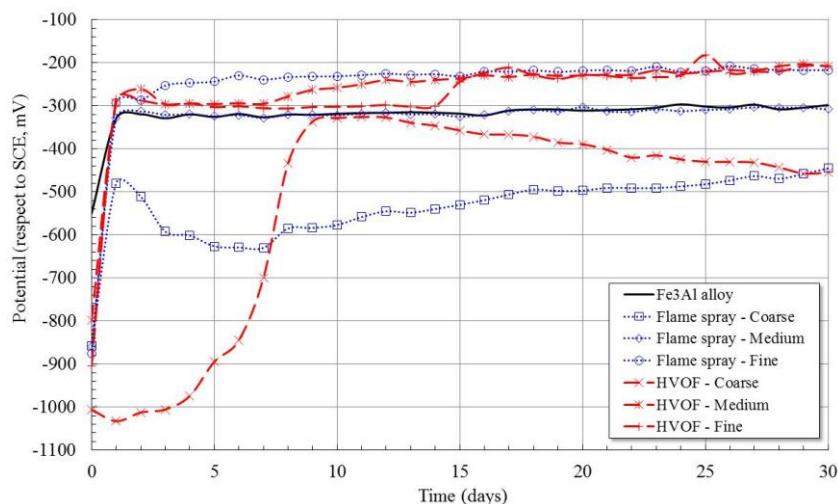


**Figure 6.**  $E_{corr}$  values measured at different testing time for the Fe<sub>3</sub>Al coatings and alloy in 1.0 M NaOH solution at 25°C.

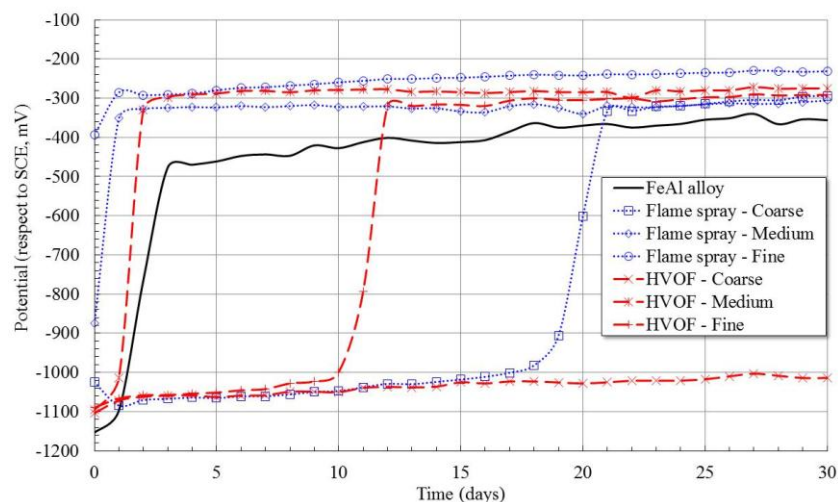


**Figure 7.**  $E_{corr}$  values measured at different testing time for the FeAl coatings and alloy in 1M NaOH solution at 25°C.

This behavior can be attributed to the growth of the oxide layer formed [37]. Moreover, coating of coarse particle size deposited by HVOF process showed a stable potential practically throughout the test, with the most active  $E_{corr}$  value of all coatings including the base alloy. This indicates a lower corrosion resistance than the other coatings.

### 3.2.3. Polarization resistance

The polarization resistance ( $R_p$ ) values were determined from the slopes of the potential vs. current plots in  $\pm 20$  mV span. It is known that once polarization resistance is determined, calculation of  $I_{corr}$  requires knowledge of the Tafel constants, and these constants can be determined from experimental polarization curves. Using the experimentally determined Tafel slopes (Tables 4-6) and the  $R_p$  values,  $I_{corr}$  values were calculated from the Stern Geary equation:

$$I_{corr} = \frac{b_a b_c}{2.303 R_p (b_a + b_c)}$$

The variation in the  $I_{corr}$  values for intermetallic alloys and coatings are given in Figure 8 and 9. In all cases, the corrosion rate data based on polarization resistance are very similar to the corrosion rates determined by the Tafel extrapolation method.

It is noted that all  $Fe_3Al$  coatings and the base alloy showed a decrease in their  $I_{corr}$  values in the first 24 hours of immersion, except coatings of coarse particle size deposited by HVOF process. Coating of coarse and fine particle size, both deposited by flame spray showed a slight increase in their  $I_{corr}$  values and these values were slightly higher than those of their base alloy. By contrast, the coatings of medium and coarse particle size both deposited by HVOF process, and the medium particle size deposited by flame spray, showed lower values than those of their base alloy. This improved performance can be associated with the presence of pre-oxidized particles deposited during the spray process, which besides being a coating defect they can be an advantage because they function as a barrier to impede the corrosion process. All coatings and intermetallic alloys exhibited a decrease in their  $I_{corr}$  value after 24 hours of immersion. Coatings of medium and fine particle size both deposited by flame spray and the fine particle size deposited by HVOF showed similar corrosion rates to that of its base alloy. Other coatings showed different behaviors with higher  $I_{corr}$  values. The corrosion rate of  $FeAl$  alloy was lower than that of  $Fe_3Al$  alloy. In general after longer immersion times, alloys and coatings with higher aluminum content had lower  $I_{corr}$  values and therefore greater corrosion resistance. It has been reported that in  $NaOH$  solutions the oxides and hydroxides both  $Fe$  and  $Al$  have protective properties and that the electrochemical behavior of pure  $Fe$  and  $Fe_{28}Al$  have the same performance [28]. This high corrosion resistance in alkaline media is due to the fact that  $OH^-$  ions react with the metallic surface and form precipitates of hydroxides, both of  $Fe$  and  $Al$  ( $Fe(OH)_2$ ,  $Al(OH)_3$ ) with protective characteristics [38, 39].

Coatings with more stable behavior were the medium particle size deposited by flame spray, and the fine particle size deposited by HVOF process. This was expected since the vast majority of

powder alloys commercially exploited for the flame spray process have a particle size similar to that used in this study. Likewise, the great majority of commercial powdered alloys for the HVOF process have a particle size similar to that used in this study.

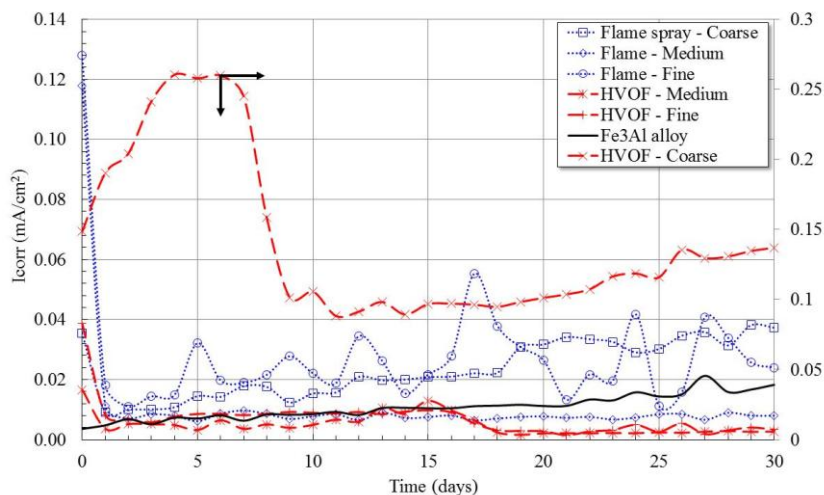


Figure 8. Corrosion current density of Fe<sub>3</sub>Al coatings.

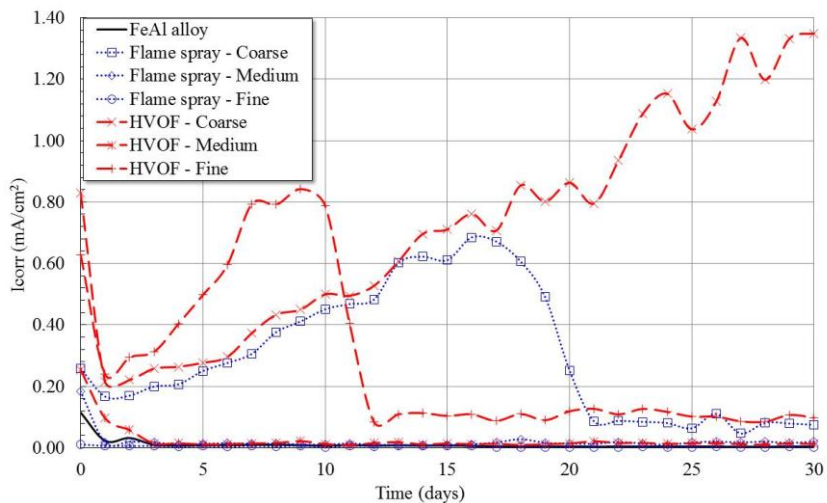


Figure 9. Corrosion current density of FeAl coatings.

#### 4. CONCLUSIONS

The microstructural characteristics of the coatings depend strongly on deposition process, as well as application parameters and the particle size used. The main differences observed when a coating is deposited from three different particle sizes are the presence of particles unfused or partially melted, oxides trapped, and the porosity of the coatings. In general, coatings and base alloys had excellent corrosion resistance in alkaline media; in particular coating with more stable behavior were

coatings of medium particle size deposited by flame spray, and coatings of fine particle size deposited by HVOF process.

## References

1. B. Szczucka-Lasota, B. Formanek, A. Hernas, K. Szymanski, *J. Mater. Process. Technol.* 164–165 (2005) 935–939.
2. T.C. Totemeier, R.N. Wright, W.D. Swank, *Intermetallics* 12 (2004) 1335–1344.
3. H. Singh, D. Puri, S. Prakash, *Metall. Mater. Trans. A* 36 (2005) 1007–1015.
4. K.R. Luer, J.N. DuPont, A.R. Marder, *Corrosion* 56 (2000) 189–198.
5. J.M. Guilemany, C.R.C. Lima, N. Cinca, J.R. Miguel, *Surf. Coat. Technol.* 201 (2006) 2072–2079.
6. J.M. Guilemany, N. Cinca, S. Dosta, C.R.C. Lima, *Intermetallics* 15 (2007) 1384–1394.
7. G. Ji, O. Elkedim, T. Grosdidier, *Surf. Coat. Technol.* 190 (2005) 406–416.
8. H. Singh, D. Puri, S. Prakash, *Surf. Coat. Technol.* 192 (2005) 27–38.
9. B.S. Sidhu, S. Prakash, *Surf. Coat. Technol.* 201 (2006) 1643–1654.
10. N. Masahashi, S. Watanabe, S. Hanada, *ISIJ International* 41 (2001) 1010–1017.
11. J.R. Blackford, R.A. Buckley, H. Jones, C.M. Sellars, D.G. McCartney, A.J. Horlock, *J. Mat. Sci.* 33 (1998) 4417–4421.
12. Y. Wang, W. Chen, *Surf. Coat. Technol.* 183 (2004) 18–28.
13. B.S. Lasota, B. Formanek, A. Hernas, *J. Mater. Process. Technol.* 164–165 (2005) 930–934.
14. Y. Wang, W. Chen, *J. Mater. Sci. Lett.* 22 (2003) 845–848.
15. A. Scrivani, S. Ianneli, A. Rossi, R. Groppetti, F. Casadei, G. Rizzi, *Wear* 250 (2001) 107–113.
16. M.B. Beardsley, *Report LLNL-JRNL-402708* April 4, 2008.
17. J.M. Guilemany, N. Cinca, S. Dosta and A.V. Benedetti, *Corros. Sci.* 51 (2009) 171–180.
18. M. M. Verdian, K. Raeissi and M. Salehi, *Corros. Sci.* 52 (2010) 1052–1059.
19. S. Frangini, A. Masci, *Surf. Coat. Technol.* 184 (2004) 31–39.
20. P. F. Tortorelli and K. Natesan, *Mater. Sci. and Eng.* A258 (1998) 115–125.
21. M.C. Garcia-Alonso, M.F. Lopez, M.L. Escudero, J.L. Gonzalez-Carrasco, D.G. Morris, *Intermetallics* 7 (1999) 185–191.
22. S.C. Deevi, V.K. Sikka, C.J. Swindeman, R. D. Seals, *J. Mater. Sci.* 32 (1997) 3315–3325.
23. B. Szczucka-Lasota, B. Formanek, A. Hernas, *J. Mater. Process. Technol.* 164–165 (2005) 930–934.
24. Pilarczyk, R. Nowosielski, M. Jodkowski, K. Labisz, H. Krztoń, *Archives of Materials Science and Engineering* 31 (2008) 29–32.
25. T. Grosdidier, A. Tidu, H.L. Liao, *Scr. Mater.* 44 (2001) 387–393.
26. T.C. Totemeier, R.N. Wright, W.D. Swank, *Metall. Mater. Trans.* 34A (2003) 2225–2231.
27. Ji Gang, Jean-Paul Morniroli, Thierry Grosdidier, *Scr. Mater.* 48 (2003) 1599–1604.
28. G. Sharma, P.R. Singh, R.K. Sharma, K. B. Gaonkar, R. V. Ramanujan, *J. Mater. Eng. Perform.* 16 (2007) 779–783.
29. Z. Xiao-lin, Y. Zheng-jun, G. Xue-dong, C. Wei, Z. Ping-ze, *Nonferrous Met. Soc. China* 19 (2009) 143–148.
30. T. Hussain, D. G. McCartney, P. H. Shipway, T. Marrocco, *Journal of Thermal Spray Technology* 20 (2011) 260–274.
31. J. Porcayo-Calderon, O. Sotelo-Mazon, V.M. Salinas-Bravo, C.D. Arrieta-Gonzalez, J.J. Ramos-Hernandez, C. Cuevas-Arteaga, *Int. J. Electrochem. Sci.* 7, (2012) 1134–1148.
32. H.C Man, Z.D Cui, T.M Yue, *Scr. Mater.* 45 (2001) 1447–1453.
33. S. Frangini, N.B. De Cristofaro, A. Mignone, J. Lascovivh and R. Giorgi, *Corros. Sci.* 39 (1997) 1431–1442.
34. N. De Cristofaro, S. Frangini and A. Mignone, *Corros. Sci.* 38 (1996) 307–315.

35. C.D. Arrieta-Gonzalez, J. Porcayo-Calderon, V.M. Salinas-Bravo, J.G. Gonzalez-Rodriguez, J.G. Chacon-Nava, *Int. J. Electrochem. Sci.* 6 (2011) 4016-4031.
36. J.M. Guilemany, J. Fernandez, N. Espallargas, P.H. Suegama, A.V. Benedetti, *Surf. Coat. Technol.* 200 (2006) 3064-3072.
37. Y. Santana-Jimenez, M. Tejera-Gil, M. Torrado-Guerra, L.S. Baltes, J.C. Mirza-Rosca, *Bulletin of the Transylvania University of Braşov* 2 (2009) 197-204.
38. S.S. Abd-El Rehim, S.S. Abd-El Haleem, S.M. Abd-El Wahaab and M. Sh. Shalaby, *Surf. Technol.* 19 (1983) 261–271.
39. M.L. Doche, J.J. Rameau, R. Durand, F. Novel-Cattin, *Corros. Sci.* 41(1999) 805-826.